Charge Transport within a Three-Dimensional DNA Nanostructure Framework

Na Lu,[†,§,⊥] Hao Pei,[†,⊥] Zhilei Ge,[†,‡] Chad R. Simmons,[‡] Hao Yan,*[,‡] and Chunhai Fan*[,†]

[†]Laboratory of Physical Biology, Shanghai Institute of Applied Physics, Chinese Academy of Sciences, Shanghai 201800, China;

[‡]The Biodesign Institute, and Department of Chemistry and Biochemistry, Arizona State University, Tempe, Arizona 85287, United States;

[§]State Key Laboratories of Transducer Technology and Science and Technology on Micro-system Laboratory, Shanghai Institute of Microsystem and Information Technology, Chinese Academy of Sciences, Shanghai 200050, China

Ⓢ *Supporting Information*

ABSTRACT: Three-dimensional (3D) DNA nanostructures have shown great promise for various applications including molecular sensing and therapeutics. Here we report kinetic studies of DNA-mediated charge transport (CT) within a 3D DNA nanostructure framework. A tetrahedral DNA nanostructure was used to investigate the through-duplex and through-space CT of small redox molecules (methylene blue (MB) and ferrocene (Fc)) that were bound to specific positions above the surface of the gold electrode. CT rate measurements provide unambiguous evidence that the intercalative MB probe undergoes efficient mediated CT over longer distances along the duplex, whereas the nonintercalative Fc probe tunnels electrons through the space. This study sheds new light on DNA-based molecular electronics and on designing high-performance biosensor devices.

There is considerable interest in using DNA as a nanoscale construction material for various applications including molecular electronics and computation.[1] The plausibility of generating DNA wires for DNA-based electronic devices has been under debate over the past two decades.[2] Evidence is accumulating that DNA duplexes have insulating properties in bulk films and on longer-length scales (e.g. >100 nm).[3,4] However, analogous to the behavior of conjugated polymers at the single-molecule level, perfectly stacked DNA duplexes were found to efficiently mediate charge transport (CT) up to 34 nm (100 base pairs), as evidenced in a recent electrochemical study of well-ordered DNA monolayers on the surface of gold electrodes.[5] In contrast to single-molecule techniques that are used to study energy migration in conjugated polymers[6] electrochemistry measures the ensemble behavior of DNA films, which is largely influenced by structural perturbation of base stacking and monolayer-packing properties.[3,7] Hence, it is critically important to preclude crowding effects (e.g., phase segregation or interstrand entanglement) in densely packed DNA films and end-to-end collision of DNA duplexes in loosely packed ones[8] that are often present in self-assembled DNA monolayers and that perturb CT at the electrode surface.

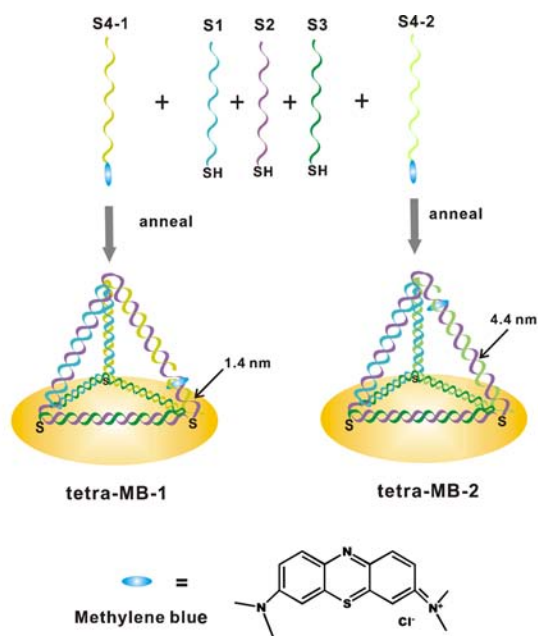Herein, we used electrochemical interrogation of a tetrahedral DNA nanostructure to provide evidence of through-duplex and through-space DNA-mediated CT. The tetrahedral DNA nanostructure[9] used here is composed of four single strands of DNA (ssDNA): S1, S2, S3, and S4. The sequences of the four strands are designed in such a way that they self-assemble into a tetrahedral frame structure with six double helical edges. Selected nucleotides along each edge were modified with thiol groups for attachment of redox molecules (methylene blue, MB, or ferrocene, Fc). Three thiol modifications per tetrahedron, one on each vertex of the 'bottom' face, were used to immobilize and anchor the structures to the surface of a gold electrode with high affinity (Figure 1).[10] DNA tetrahedra were synthesized with high yield (>85%, Figure S2, Supporting Information [SI]), even with thiol modifications.

DNA tetrahedra are ideal molecular scaffolds because they possess high mechanical rigidity and structural stability.[11] These features are particularly important for electrochemical applications. Previous structural characterization of double helices within a DNA monolayer revealed that they predominantly adopt an upright orientation, tilted relative to the electrode surface.[12] However, the local disorder in the monolayer and potential end-to-end collision with the electrode surface that are the result of the dynamic motion of the DNA has made it a difficult system to study. Surface-confined three-dimensional (3D) DNA tetrahedra present an unprecedented opportunity for studying DNA-mediated CT due to their stability, rigidity, and well-defined structure and orientation at the surface.[10]

First, we conjugated the redox molecule MB to two different positions on a DNA tetrahedron and examined the electrochemical kinetics of DNA-mediated CT. In one design (tetra-MB-1), MB was located four nucleotides from the Au surface (5′-MB-TGAA-3′, estimated to be ~1.4 nm away from the electrode). In the second design (tetra-MB-2), MB was 13 nucleotides (5′-MB-TCCTAAGTCTGAA-3′, or ~4.4 nm) above the electrode surface. Cyclic voltammetric (CV) analysis of both structures revealed a pair of redox peaks representing an exchange of electrons between MB and the Au electrode (Figure S3, SI). While the CV peaks were clearly visible, the peak amplitudes were too small to perform a detailed analysis of the CT processes, likely because of the low surface density of the bulky nanostructures.

Figure 1. Assembly of electrochemically active DNA tetrahedra. Tetrahedra were assembled from three thiolated 55-mer strands (S1–S3) and a 57-mer MB-labeled strand (S4-1 or S4-2). Tetrahedra were anchored to the electrode surface by gold–thiol interactions between thiolated vertices and the gold electrode. MB was incorporated into the tetrahedra at predefined distances away from the Au surface, i.e. tetra-MB-1 (1.4 nm) and tetra-MB-2 (4.4 nm).

Next, we used alternating current voltammetry (ACV) to analyze the structures. ACV is more sensitive than CV for probing low-density species at an electrode surface.[13] Analysis of tetra-MB-1 and tetra-MB-2 revealed similar ACV curves with peaks centered at −0.30 V (Figure 2a). The surface density of MB was obtained using eq 1,[14] where I_{avg} (E_0) is the average peak, n is the number of electrons transferred per redox event, f is the frequency of the applied alternating current (ac) voltage perturbation, F is Faraday constant, R is the universal gas

Figure 2. (a) ACVs at 5 Hz for tetra-MB-1 (1.4 nm, red) and tetra-MB-2 (4.4 nm, blue). (b) Plot of I_p/I_b vs log(frequency) for tetra-MB-1 and tetra-MB-2.

constant, T is the temperature in Kelvin, E_{ac} is the peak amplitude, and N_{tot} is the total molar quantity of the redox species.

$$I_{avg}(E_0) = 2nfFN_{tot} \tanh(nFE_{ac}/2RT) \tag{1}$$

The calculated surface density of each structure was ∼3.2 × 10^{12} tetrahedra·cm^{-2} (<10% monolayer), which corresponds to approximately 5.6 nm between structures. The low surface density prevents intermolecular interactions and accounts for the small CV peak amplitudes that were observed.

CT rate constants are obtained by plotting the ratio of the ACV peak current to the background current (I_p/I_b) vs variable ACV frequency.[13] After analyzing the plots, we obtained the following CT rate constants: $k_{tetra-MB-1}$ = 15 ± 2 s^{-1} and $k_{tetra-MB-2}$ = 15 ± 3 s^{-1} (Figure 2b). Similar rates were also obtained by kinetic studies with CV (see Figure S7 in SI). Clearly, the position of MB in the DNA tetrahedron did not affect the peak current or the CT rate. This through-duplex CT is explained by a compound hole-hopping mechanism involving $G^+···G$ superexchange mediation via short $(T-A)_n$ bridges in the duplex.[15]

In a control study, when MB-labeled, nonthiolated ssDNA was physically adsorbed on Au, the resulting CV peaks were more intense with significantly smaller peak separation (∼14 mV) than for the DNA tetrahedra-modified surface (Figure S4b, SI), characteristic of CV behaviors of physically adsorbed MB.[5] Similarly, ACV studies revealed that the CT rate (180 ± 11 s^{-1}) was 12-fold faster than was observed for the DNA tetrahedra (Figure 2b). The distinct differences between the electrochemical kinetic profile of the tetrahedron sample and the direct CT results (MB-labeled, nonthiolated ssDNA) suggest that the framework of the tetrahedra prevents direct collision between MB and the electrode surface. Although faster transfer kinetics was observed for the MB-labeled ssDNA, it does not necessarily mean that through-duplex CT is slower than direct-contact CT; the kinetic barrier is governed by the alkylthiol linker between the thiol and nucleotides (∼1 nm). By extrapolation to the zero linker-length, the rate of through-the-stack CT should be as large as 10^8–10^9 s^{-1}.[7]

We also prepared high-density, thiolated, double-stranded DNA (dsDNA) monolayers (20 or 57 base pairs long) on the Au surface (Figure S5, SI). While the peak currents were much larger than those obtained at the tetrahedral surface, the CT kinetics were nearly the same with k_{20} = 13 ± 3 s^{-1}, and k_{57} = 12 ± 2 s^{-1} (Figure S5c, SI). These rate constants are in the same order of magnitude as those of a previous report (39 s^{-1}) that used similar dsDNA monolayers.[5] The similarity in kinetics suggests that the density of the DNA monolayer is not a critical factor for through-duplex CT.

We introduced a one-base-pair mismatch in one edge of the tetrahedron to determine if charge passes through the DNA double helices via stacked nucleobases (Figure 3a). The peak nearly disappeared in the CV spectra (Figure S6, SI), and the ACV current was largely attenuated by the introduction of the mismatch (Figure 3b). The CT kinetics for the mismatched tetrahedron (tetra-MB-MM, k_{MM} = 3 ± 1 s^{-1}) was 5-fold slower than for the fully complementary one (tetra-MB-WM, k_{WM} = 15 ± 3 s^{-1}) (Figure 3c). Clearly, through-duplex CT is very sensitive to perturbation of π-stacking in the duplex.[16]

Finally, we studied CT of Fc, a nonintercalative redox probe that does not intercalate between the stacked nucleobases of the double helix.[17] Fc was attached to the bottom (0.8 nm above the Au surface), middle (3.1 nm above), and top (5.7 nm
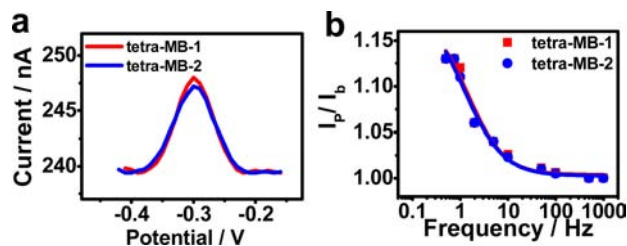
13149

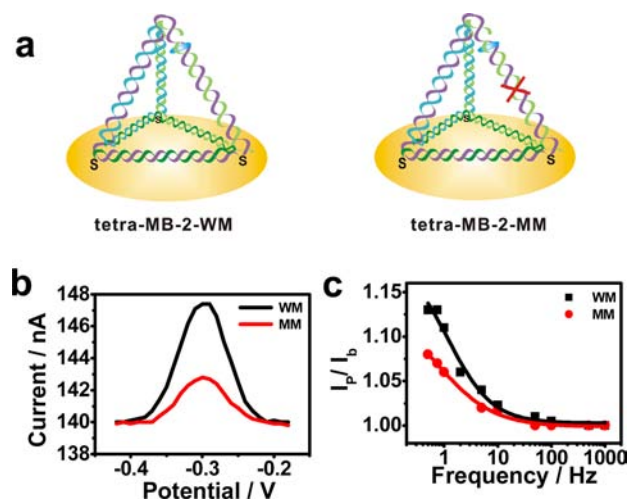dx.doi.org/10.1021/ja302447r | *J. Am. Chem. Soc.* 2012, 134, 13148–13151

Figure 3. (a) Perfectly complementary (tetra-MB-2-WM) and one-base-pair mismatched (tetra-MB-2-MM) tetrahedra. (b) ACVs of tetra-MB-2-WM (black) and tetra-MB-2-MM (red). Frequency = 5 Hz, ac amplitude = 25 mV. (c) Plots of I_p/I_b vs log(frequency) for tetra-MB-2-WM (black) and tetra-MB-2-MM (red).

above) of the DNA tetrahedra (tetra-Fc, Figure 4a). The mentioned distances between Fc-tagged nucleobases and the
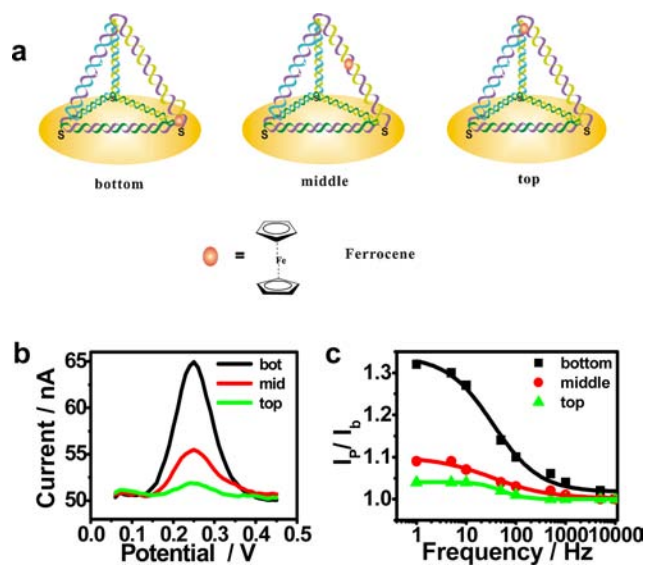

Figure 4. (a) Fc attached to the bottom, middle, and top of the DNA tetrahedra. (b) ACVs of Fc labeled at the bottom (black), middle (red), and top (green) of the tetrahedra. Frequency = 1 Hz; amplitude = 25 mV. (c) Plot of I_p/I_b vs log(frequency) for Fc labeled at the bottom (black), middle (red), and top (green) of the tetrahedra.

electrode surface are based on the length of the methylene spacer (0.77 Å) and the number of base pairs in the double helices (3.4 Å/base). However, since Fc is tagged to nucleobases via a soft, six-carbon linker that makes it dangle at the tetrahedral nanostructure, the real distance between Fc and the electrode cannot be estimated. We observed a pair of redox peaks for the tetrahedron with Fc attached to the bottom surface, while the other Fc-labeled tetrahedra did not exhibit prominent CV peaks (Figure S8, SI). For the former case, the midpoint potential was ~0.22 V, with 14 mV separation between peaks. We observed well-defined ACV peaks centered

at 0.250 V for all three designs (Figure 4b). The CT rate constants calculated from plots of I_p/I_b versus ac frequency are: $k_{bottom} = 445 \pm 21$ s^{-1}, $k_{middle} = 365 \pm 13$ s^{-1}, and $k_{top} = 118 \pm 9$ s^{-1} (Figure 4c), characteristic of distance-dependent through-space CT.

An upward monolayer orientation is essential for DNA-mediated CT studies. However, previous reports have shown that loosely packed dsDNA monolayers have distinct "island" morphologies in which the DNA is free to bend and strike at the gold surface.[18] The introduction of mechanically rigid and structurally stable DNA nanostructures addresses this issue, providing an ideal platform for studying CT of redox probes. We provided clear evidence that intercalative MB transports electrons via efficient mediation of DNA duplexes. In contrast, Fc is a nonintercalative molecule that cannot be efficiently coupled to the stacked nucleobases of the double helix and exhibits typical through-space CT that is strongly dependent on the distance. The results suggest that DNA nanostructures can be used for the rational design of switchable DNA nanodevices for electronic, biosensor, and computational applications.

Oligonucleotides were synthesized and purified by TaKaRa Inc. (Dalian, China); the sequences can be found in the SI. To form DNA tetrahedra, equimolar amounts of the four constituent oligonucleotides were combined in TM buffer (10 mM Tris-HCl, 35 mM MgCl$_2$, pH 8.0). The reaction mixture was maintained at 95 °C for 3 min and then was cooled to 4 °C over 3 min.[10]

Prior to measurement, electrodes were thoroughly cleaned according to a well-established protocol.[19] The clean electrodes were incubated with 0.1 μM tetra-MB or 1 μM Fc-tetra in TM buffer (10 mM tris-HCl, 35 mM MgCl$_2$, and 1 mM TCEP, pH 8.0) overnight at room temperature. Modified electrodes were subsequently treated with 1 mM MCH for one hour. Electrochemical measurements were performed with a CHI 630b electrochemical workstation (CH Instruments Inc., Austin, TX, U.S.A.) and a conventional three-electrode configuration.

■ ASSOCIATED CONTENT

Ⓢ Supporting Information

Materials and protocols, additional figures. This material is available free of charge via the Internet at http://pubs.acs.org.

■ AUTHOR INFORMATION

Corresponding Author
fchh@sinap.ac.cn; hao.yan@asu.edu

Author Contributions
[⊥]These authors contributed equally to this work

Notes
The authors declare no competing financial interest.

■ ACKNOWLEDGMENTS

■ REFERENCES

(1) Omabegho, T.; Sha, R.; Seeman, N. C. *Science* **2009**, *324*, 67. Lund, K.; Manzo, A. J.; Dabby, N.; Michelotti, N.; Johnson-Buck, A.; Nangreave, J.; Taylor, S.; Pei, R.; Stojanovic, M. N.; Walter, N. G.; Winfree, E.; Yan, H. *Nature* **2010**, *465*, 206. Gu, H.; Chao, J.; Xiao, S.-J.; Seeman, N. C. *Nature* **2010**, *465*, 202. Qian, L.; Winfree, E. *Science* **2011**, *332*, 1196.

(2) Murphy, C. J.; Arkin, M. R.; Jenkins, Y.; Ghatlia, N. D.; Bossmann, S. H.; Turro, N. J.; Barton, J. K. *Science* **1993**, *262*, 1025. Braun, E.; Eichen, Y.; Sivan, U.; Ben-Yoseph, G. *Nature* **1998**, *391*, 775. Porath, D.; Bezryadin, A.; de Vries, S.; Dekker, C. *Nature* **2000**, *403*, 635. Fink, H. W.; Schonenberger, C. *Nature* **1999**, *398*, 407. Kasumov, A. Y.; Kociak, M.; Gueron, S.; Reulet, B.; Volkov, V. T.; Klinov, D. V.; Bouchiat, H. *Science* **2001**, *291*, 280.

(3) Genereux, J. C.; Barton, J. K. *Chem. Rev.* **2010**, *110*, 1642. Gorodetsky, A. A.; Buzzeo, M. C.; Barton, J. K. *Bioconjugate Chem.* **2008**, *19*, 2285.

(4) Storm, A. J.; van Noort, J.; de Vries, S.; Dekker, C. *Appl. Phys. Lett.* **2001**, *79*, 3881.

(5) Slinker, J. D.; Muren, N. B.; Renfrew, S. E.; Barton, J. K. *Nature Chem.* **2011**, *3*, 228.

(6) Vogelsang, J.; Adachi, T.; Brazard, J.; Vanden Bout, D. A.; Barbara, P. F. *Nat. Mater.* **2011**, *10*, 942. Bolinger, J. C.; Traub, M. C.; Adachi, T.; Barbara, P. F. *Science* **2011**, *331*, 565.

(7) Drummond, T. G.; Hill, M. G.; Barton, J. K. *J. Am. Chem. Soc.* **2004**, *126*, 15010.

(8) Cash, K. J.; Ricci, F.; Plaxco, K. W. *J. Am. Chem. Soc.* **2009**, *131*, 6955. White, R. J.; Plaxco, K. W. *Anal. Chem.* **2009**, *82*, 73.

(9) Goodman, R. P.; Berry, R M.; Turberfield, A. *J. Chem. Commun.* **2004**, 1372. Goodman, R. P.; Schaap, I. A. T.; Tardin, C. F.; Erben, C. M.; Berry, R. M.; Schmidt, C. F.; Turberfield, A. J. *Science* **2005**, *310*, 1661.

(10) Pei, H.; Lu, N.; Wen, Y.; Song, S.; Liu, Y.; Yan, H.; Fan, C. *Adv. Mater.* **2010**, *22*, 4754. Pei, H.; Wan, Y.; Li, J.; Hu, H.; Su, Y.; Huang, Q.; Fan, C. *Chem. Commun.* **2011**, *47*, 6254. Wen, Y.; Pei, H.; Wan, Y.; Su, Y.; Huang, Q.; Song, S.; Fan, C. *Anal. Chem.* **2011**, *83*, 7418.

(11) Mitchell, N.; Schlapak, R.; Kastner, M.; Armitage, D.; Chrzanowski, W.; Riener, J.; Hinterdorfer, P.; Ebner, A.; Howorka, S. *Angew. Chem., Int. Ed.* **2009**, *48*, 525.

(12) Gorodetsky, A. A.; Barton, J. K. *Langmuir* **2006**, *22*, 7917.

(13) Creager, S. E.; Wooster, T. T. *Anal. Chem.* **1998**, *70*, 4257.

(14) Sumner, J. J.; Weber, K. S.; Hockett, L. A.; Creager, S. E. *J. Phys. Chem. B* **2000**, *104*, 7449.

(15) Wagenknecht, H.-A.; Rajski, S. R.; Pascaly, M.; Stemp, E. D. A.; Barton, J. K. *J. Am. Chem. Soc.* **2001**, *123*, 4400. Giese, B.; Amaudrut, J.; Kohler, A. K.; Spormann, M.; Wessely, S. *Nature* **2001**, *412*, 318. Park, M. J.; Fujitsuka, M.; Kawai, K.; Majima, T. *J. Am. Chem. Soc.* **2011**, *133*, 15320. Kawai, K.; Hayashi, M.; Majima, T. *J. Am. Chem. Soc.* **2012**, *134*, 4806. Conron, S. M. M.; Thazhathveetil, A. K.; Wasielewski, M. R.; Burin, A. L.; Lewis, F. D. *J. Am. Chem. Soc.* **2010**, *132*, 14388.

(16) Boon, E. M.; Ceres, D. M.; Drummond, T. G.; Hill, M. G.; Barton, J. K. *Nat. Biotechnol.* **2000**, *18*, 1096. Slinker, J. D.; Muren, N. B.; Gorodetsky, A. A.; Barton, J. K. *J. Am. Chem. Soc.* **2010**, *132*, 2769.

(17) Fan, C.; Plaxco, K. W.; Heeger, A. J. *Proc. Natl. Acad. Sci. U.S.A.* **2003**, *100*, 9134.

(18) Uzawa, T.; Cheng, R. R.; White, R. J.; Makarov, D. E.; Plaxco, K. W. *J. Am. Chem. Soc.* **2010**, *132*, 16120.

(19) Zhang, J.; Song, S.; Wang, L.; Pan, D.; Fan, C. *Nat. Protoc.* **2007**, *2*, 2888.